Semiclassical description of nuclear dynamics in x-ray emission of water

M. P. Ljungberg,[1] A. Nilsson,[1,2] and L. G. M. Pettersson[1]
[1]*FYSIKUM, Stockholm University, AlbaNova, S-106 91 Stockholm, Sweden*
[2]*Stanford Synchrotron Radiation Lightsource, P.O. Box 20450, Stanford, California 94309, USA*
(Received 12 August 2010; revised manuscript received 3 October 2010; published 14 December 2010)

In this paper we present a semiclassical approximation to the Kramers-Heisenberg formula for calculating x-ray emission (XE) spectra, including vibrational effects. We compare the method to the quantum Kramers-Heisenberg formula for a test system consisting of a model water dimer where the hydrogen-bond donor is core ionized and obtain excellent agreement. In the semiclassical approach we average spectra from classical trajectories where the core-hole-induced dynamics is performed with initial conditions sampling the quantum zero-point position and momentum probability distributions in the O-H vibration. We find very similar time evolution of the squared quantum wave packet compared to the probability distribution under classical dynamics until the proton interacts with the next water. We compare our semiclassical approach with other methods to compute the XES spectra of water that have been used in the past and conclude that our approach gives superior results while requiring the same computational effort.

DOI: 10.1103/PhysRevB.82.245115 PACS number(s): 78.70.En, 71.15.Qe, 79.60.Cn

I. INTRODUCTION

Core-hole-induced dynamics has become an issue for the interpretation of recently reported x-ray emission (XE) spectra on liquid water where, in the lone-pair region, two well-resolved sharp peaks appear.[1–3] These have been interpreted either as indicative of two specific structural motifs in the liquid[2,4]—thus strongly questioning the picture of liquid water as a continuous distribution around mainly tetrahedral coordination—or as due to ultrafast core-hole-induced dissociation giving emission from intact H_2O and fully dissociated OH,[1,5,6] supporting the traditional picture. Clearly the creation of the core-hole represents a strong perturbation which induces significant vibrational broadening and dynamics on the core-ionized potential-energy surface (PES),[5,7,8] but can the two peaks be explained as due to dissociation? In Refs. 2 and 9 experimental observations were given against this interpretation and in Refs. 9 and 10 the importance of the release of zero-point energy and of a sampling of the zero-point position distribution when simulating excited state dynamics on a repulsive PES was pointed out. In Refs. 5 and 6 it was, on the other hand, claimed that only classical initial conditions should be used in classical dynamics, even when simulating the effects of vibrational broadening and dynamics on an inherently quantum system, such as hydrogen-bonded liquid water. A first step in addressing these issues is to investigate the different approximate methods of calculating XES for a small well-defined test system where a more accurate calculation can be done for comparison.

A rigorous way of taking vibrational broadening and interference effects into account when computing XES is to use the Kramers-Heisenberg (KH) formula.[11,12] Here a full set of vibrational eigenstates must be determined for each electronic state making the calculations cumbersome. A way to avoid this is to go to the time domain which leads to wave-packet propagation techniques.[11,13,14] However, the full PES of all electronic states must be computed in these approaches, which makes them impractical for systems with many degrees of freedom. It is therefore essential to develop approximate but still reliable schemes when dealing with condensed phase systems such as liquid water or ice. Note an important feature of liquid water, namely, that for an H-bonded OH the core-ionized state PES is dissociative along the OH stretch but still bounded by the receiving molecule. Due to the small spacing between vibrational levels in the intermediate PES the scattering of x rays is strongly affected by quantum interference, so-called lifetime vibrational interference.[15] Thus, when trying to simplify the strict quantum scheme of simulations, we should keep this interference effect in our semiclassical method.

In the present paper we compare different approximate methods of computing XES, including those used in Refs. 9 and 10, to the KH method for a one-dimensional test system consisting of a model water dimer with either the bonded or the nonbonded hydrogen free to move. We develop a method, the semiclassical KH (SCKH) method, which is found to give very good agreement with KH, in contrast to the other methods investigated. In the SCKH method the electronic degrees of freedom are treated quantum mechanically while the nuclear motion is treated classically. This is realized by writing the KH formula in the time domain and replacing the quantum ensemble average by an average over classical trajectories on the core-hole state potential with initial conditions sampled from a quantum distribution in both position and momentum. This method is in the spirit of Refs. 16–18 where the time-ordered exponential is used to rewrite the time development on a single PES and the semiclassical approximation is obtained by letting the operators in the Heisenberg representation go to classical quantities. In the present paper we start our derivation of the XES cross section directly from the Kramers-Heisenberg formula instead of from response functions[17,18] and consider an excitation process that ionizes an electron which further simplifies our formulas. As the excitation process in our case changes the PES significantly we need to start our trajectories from the time of the excitation; we cannot simply average trajectories from a ground-state simulation as is usually done in similar methods. Finally, due to hydrogen being a light element, quantum effects are important and consequently we have

 ©2010 The American Physical Society

used quantum initial conditions for the classical trajectories and calibrated against full wave-packet dynamics with excellent agreement on the time scale relevant for XES.

Unlike the KH formula, the SCKH method can easily be generalized to include more degrees of freedom which makes it practical for more general systems of larger size. A full-dimensional calculation with a realistic model of water is, however, a separate investigation altogether and outside the scope of this paper.

II. METHODS

A. Kramers-Heisenberg formula

For a nonresonant transition the Kramers-Heisenberg formula is (see derivation in Appendix A)

$$\sigma(\omega') = \sum_f \left| \sum_n \frac{\langle f|D'|n\rangle\langle n|D|i\rangle}{\omega' - E_{nf} + i\Gamma} \right|^2, \tag{1}$$

where i denotes the initial state, n the intermediate states and f the final states, $E_{nf}=E_n-E_f$ is the energy difference between intermediate and final states, and Γ is the half-width-at-half-maximum (HWHM) lifetime broadening. ω' is the frequency of the emitted photon. D' is the dipole operator of the emission process $D'=\mathbf{E}\cdot\Sigma_i\mathbf{r}_i$ with $\mathbf{E}$ the polarization of the emitted radiation and the sum is over all electronic coordinates. D is the dipole operator of the incoming radiation and is written similarly. In the nonresonant case matrix elements of D are insensitive to both the polarization direction and the intermediate state;[19] in our numerical simulations we will therefore set D to unity although it will be present throughout the derivations.

By the Born-Oppenheimer (B-O) approximation the wave functions are written as a product of an electronic wave function (parametrically dependent on the nuclear coordinates) and a nuclear wave function

$$|i\rangle = |\varphi_I(r;R)\rangle|\chi_{Ii}(R)\rangle \equiv |I\rangle|i_I\rangle, \tag{2}$$

where i_I denotes the ith vibrational state on the Ith electronic state PES. An operator can then be written in terms of the electronic states as $\hat{O}=\Sigma_{IJ}|I\rangle O_{IJ}(R)\langle J|$ with $O_{IJ}(R)=\langle I|\hat{O}|J\rangle$. $O_{IJ}(R)$ is thus a matrix element of the operator with respect to electronic states but still an operator with respect to nuclear states, as indicated by the R dependence. A typical full matrix element appears as

$$\langle i_I|\langle I|\hat{O}|J\rangle|j_J\rangle = \langle i_I|O_{IJ}|j_J\rangle. \tag{3}$$

Ignoring purely vibrational transitions the electronic dipole operator is

$$D = \sum_{I\neq J} |I\rangle D_{IJ}(R)\langle J|. \tag{4}$$

Putting this into Eq. (1) gives

$$\sigma(\omega') = \sum_F \sum_{f_F} \left| \sum_{n_N} \frac{\langle f_F|D'_{FN}|n_N\rangle\langle n_N|D_{NI}|i_I\rangle}{\omega' - E_{n_N f_F} + i\Gamma} \right|^2, \tag{5}$$

where, e.g., D_{FN} is given by $D_{FN}(R)=\langle F|\hat{D}|N\rangle$. Equation (5) will serve as our benchmark when evaluating the semiclassical approximation and other methods.

B. Semiclassical approximation to the Kramers-Heisenberg formula

For the semiclassical approximation to the Kramers-Heisenberg formula (SCKH) we want to treat the nuclear degrees of freedom in the time domain and use the relationship

$$\frac{1}{\omega' - E_{n_N f_F} + i\Gamma} = -i\int_{-\infty}^{\infty} dt\,\theta(t) e^{-iE_{n_N f_F}t - \Gamma t} e^{i\omega' t} = -i\int_0^{\infty} dt e^{-iE_{n_N f_F}t - \Gamma t} e^{i\omega' t}. \tag{6}$$

By using $e^{-iE_{n_N}t}|n_N\rangle = e^{-iH_N t}|n_N\rangle$ and $\langle f_F|e^{iE_{f_F}t} = \langle f_F|e^{iH_F t}$, where $H_N=\langle N|\hat{H}|N\rangle$ is the vibrational Hamiltonian on the B-O PES of the electronic state N (similar for H_F), this leads to

$$\sigma(\omega') = \sum_F \sum_{f_F} \left| -i\int_0^{\infty} dt \sum_{n_N} \langle f_F|D'_{FN}|n_N\rangle \times \langle n_N|D_{NI}|i_I\rangle e^{-iE_{n_N f_F}t - \Gamma t} e^{i\omega' t} \right|^2 \tag{7}$$

$$= \sum_F \sum_{f_F} \left| -i\int_0^{\infty} dt \sum_{n_N} \langle f_F|e^{iH_F t} D'_{FN} e^{-iH_N t}|n_N\rangle \times \langle n_N|D_{NI}|i_I\rangle e^{-\Gamma t} e^{i\omega' t} \right|^2. \tag{8}$$

Expanding the square and using the resolution of the identity, $\Sigma|i\rangle\langle i|=1$, to remove the sums over intermediate and final vibrational states we get

$$= \sum_F \langle i_I| \int_0^{\infty} dt D^+_{NI} e^{iH_N t'} D'^+_{FN} e^{-iH_F t'} e^{-\Gamma t'} e^{-i\omega' t'} \times \int_0^{\infty} dt e^{iH_F t} D'_{FN} e^{-iH_N t} D_{NI} e^{-\Gamma t} e^{i\omega' t}|i_I\rangle \tag{9}$$

$$= \sum_F \langle i_I|D^+_F(\omega')D_F(\omega')|i_I\rangle = \sum_F \mathrm{Tr}[D^+_F(\omega')D_F(\omega')\rho] \tag{10}$$

with

$$D^+_F(\omega') = \int_0^{\infty} dt D^+_{NI} e^{iH_N t} D'^+_{FN} e^{-iH_F t} e^{-\Gamma t'} e^{-i\omega' t}. \tag{11}$$

ρ is the density matrix. Writing a trace instead of an expectation value generalizes the expression to also describe en-

sembles. In this expression we have time evolutions on both intermediate and final states. To avoid this we rewrite the final-state time-evolution operator[18]

$$e^{-iH_F t} = e^{-iH_N t} e_+^{-i\int_0^t [H_F(\tau)-H_N(\tau)]d\tau}, \tag{12}$$

where the (positive) time-ordered exponential of a Hermitian operator A is defined as[18]

$$e_+^{-i\int_{t_0}^t A(\tau)d\tau} = 1 + \sum_{n=1}^{\infty} (-i)^n \int_{t_0}^{t} d\tau_n \int_{t_0}^{\tau_n} d\tau_{n-1} \ldots \times \int_{t_0}^{\tau_2} d\tau_1 A(\tau_n) A(\tau_{n-1}) \ldots A(\tau_2) A(\tau_1)$$

and the Hamiltonian operators are written in the Heisenberg representation as

$$H_F(t) - H_N(t) = e^{iH_N t}(H_F - H_N)e^{-iH_N t}. \tag{13}$$

Here everything moves on the intermediate PES and we can rewrite Eq. (11) in the Heisenberg representation with $D_{FN}(t) = e^{iH_N t} D_{FN} e^{-iH_N t}$

$$D_F^+(\omega') = \int_0^{\infty} dt D_{NI}^+(0) D_{FN}'^+(t) e_+^{-i\int_0^t [H_F(\tau)-H_N(\tau)]d\tau} e^{-\Gamma t} e^{-i\omega' t}. \tag{14}$$

As of yet no approximations have been introduced; Eq. (14) in combination with Eq. (10) is just a reformulation of Eq. (5). We now make the semiclassical approximation: the time evolution is treated classically and the trace goes to a sum of classical trajectories on the intermediate PES but started from a sampling of the ground-state quantum distribution of distance and momentum. The time-ordered exponential goes to a normal exponential with the intermediate- and final-state energies in the place of the Hamiltonians.

$$\sigma^{class}(\omega') = \sum_{traj} \sum_{F} |D_F^{+class}(\omega')|^2, \tag{15}$$

$$D_F^{+class}(\omega') = \int_0^{\infty} dt D_{NI}^+(0) D_{FN}'^+(t) e^{-i\int_0^t (E_F(\tau)-E_N(\tau))d\tau} e^{-\Gamma t} e^{-i\omega' t}. \tag{16}$$

Equations (15) and (16) are the final expressions for the SCKH approximation. In the present case we have sampled the initial conditions such that all trajectories have equal probability, which eliminates the need to include an additional weight factor for each trajectory in Eq. (15).

C. Two-step approximations

The KH formula takes vibrational effects from the intermediate and final states into account in one step, thus including the interference of the intermediate-state wave functions.[15] This so-called lifetime vibrational interference (LVI) (Ref. 15) is of crucial importance for dissociative core excited states due to zero-energy spacing between continuum nuclear states; in the present case, considering the water dimer model, the PES is dissociative but bounded, leading to LVI effects between closely spaced vibrational levels in the potential well between the two oxygens.[20] Simplified methods of calculating XES can still be obtained by using a two-step approach where the absorption and emission processes are treated separately.[21] The simplest approximation can be termed the vertical approximation (VA) and results from assuming the intermediate- and final-state vibrational wave functions to be position eigenstates (Dirac delta functions), that is $|f_F\rangle \rightarrow |R\rangle$ and $|n_N\rangle \rightarrow |R'\rangle$. The sums over vibrational states go to integrals.

$$\sigma(\omega') = \sum_F \int dR \left| \int dR' \frac{\langle R|D_{FN}'|R'\rangle\langle R'|D_{NI}|i_I\rangle}{\omega' - [E_N(R') - E_F(R)] + i\Gamma} \right|^2. \tag{17}$$

Since $\langle R|D_{FN}|R'\rangle = D_{FN}(R)\delta(R-R')$ all the cross terms vanish and inserting $\int dR''|R''\rangle\langle R''|$ between D_{NI}' and $|i_I\rangle$ results in

$$\sigma(\omega') = \sum_F \int dR \frac{|D_{FN}'(R)|^2 |D_{NI}(R)|^2 |\chi_i(R)|^2}{[\omega' - E_{NF}(R)]^2 + \Gamma^2}, \tag{18}$$

where $\chi_i(R) = \langle R|i_I\rangle$ is the ground-state vibrational wave function. If D_{NI} is set to unity, this corresponds to summing the Fermi's golden rule expression for transitions from intermediate to final states calculated for point R, weighted with the ground-state vibrational distribution. The VA [Eq. (18)] clearly cannot handle dissociation since only geometries near the ground-state geometry are sampled. To solve this problem one should use strict quantum theory of x-ray Raman scattering, which treats the scattering through the dissociative intermediate states rigorously.[22] However, this strict wave-packet technique only allows treating rather small molecules. Keeping in mind the intended application to large systems, such as realistic models of liquid water, we need to introduce reasonable approximations.

Attempts to include the dissociative effects within the two-step approach have been made in several studies[2,5–10] where the latest efforts by Odelius,[5,6] Tokushima *et al.*,[2,9] and Pettersson *et al.*[10] are all equivalent except for a few important points described below. As in the SCKH method presented here, classical trajectories on the core-hole PES are used with either classical[5,6] or quantum[2,9,10] initial conditions. The spectra are calculated at the instantaneous geometry at each time step using Fermi's golden rule (ignoring the D_{NI}' absorption matrix element)

$$\sigma_{traj}[\omega', R(t_i)] = \sum_F \frac{|D_{FN}'[R(t_i)]|^2}{\{\omega' - E_{NF}[R(t_i)]\}^2 + \Gamma^2} \tag{19}$$

and summed together with an exponential damping factor corresponding to the lifetime, τ, of the core hole, and averaging over the trajectories

$$\sigma_{tot}(\omega') = \sum_{traj} \sum_i \sigma_{traj}[\omega', R(t_i)] e^{-t_i/2\tau}. \tag{20}$$

We denote this method spectra summed over classical trajectories (SSCT). The initial step, calculated for time zero, corresponds to the VA if the quantum initial position distribution

is sampled. In earlier work a Gaussian broadening has been used instead of a Lorentzian.

The lifetime τ is commonly defined as $\hbar/\Gamma'$, where Γ' is the full width at half maximum (FWHM) Lorentzian lifetime broadening (we use the prime to distinguish the FWHM from the Γ we use that corresponds to the HWHM). In Ref. 23 the FWHM of the lifetime broadening of O_2 has been reported as 0.18 eV, giving a lifetime of 3.6 fs according to this definition and in Ref. 24 a lifetime of ~3 fs was given based on a lifetime width of 0.15 eV. In earlier work[2,5,7–10] an exponential factor $e^{-t_i/\tau}$ has been used with this lifetime, which corresponds to the decrease in the population of a certain state, see Appendix B. To compare with the earlier work we show spectra computed with $e^{-t_i/\tau}$ as well as $e^{-t_i/2\tau}$ which is consistent with the lifetime of the KH formula written in the time domain. In the latter case the lifetime is effectively twice that which has been used in previous work.[2,7–10]

A generalization of the methods described above is to use full wave-packet quantum dynamics to do the time propagation and summing spectra for different times according to the probability $|\chi_N(R,t)|^2$, i.e., the wave packet squared, and furthermore weighted with the exponentially decreasing lifetime factor. We call this the spectra summed over wave-packet probability (SSWPP) method

$$\sigma(\omega') = \sum_F \sum_i \sum_j \frac{|D_{FN}(R_j)|^2 |\chi_N(R_j,t_i)|^2}{[\omega' - E_{NF}(R_j)]^2 + \Gamma^2} e^{-t_i/2\tau}. \quad (21)$$

Here we need $|\chi_N(R,t)|^2$, which is obtained from quantum wave-packet dynamics on the core-hole PES, see Sec. II F below.

D. Electronic structure calculations and core-hole-induced trajectories

Calculations were performed for a water dimer with the O-O distance constrained to 2.75 Å but with all other geometrical parameters fully optimized; this is a realistic O-O distance for the dimer as a local model of liquid water and ice. At this distance and distances shorter than the experimental gas-phase dimer distance of 2.978 Å,[25] the PES for the H-bonded hydrogen in the nonresonant core-hole state is dissociative. In earlier related work[26,27] an optimized O-O distance of 3.13 Å in the $(H_2O)_2$ dimer was used which introduced an artificial barrier and too slow dynamics in the simulated core-hole-induced proton-transfer reaction. In order to have a direct comparison between a quantum treatment of vibrational effects on a precomputed PES and core-hole-induced trajectories with *ab initio* forces the forces were projected on the same direction along which the PES was computed (O-H···O for the H-bonded OH and O-H for the non-H-bonded); the dynamics was thus constrained to be on the same PES as for the full KH calculations. All electronic structure calculations were made with the STOBE density-functional theory code[28] using the PBE gradient-corrected functional[29] and the IGLO-III all-electron basis set of Kutzelnigg *et al.*[30] for the H-bond-donating oxygen while the accepting oxygen was described using an effective core potential (ECP) (Ref. 31) which simplifies the definition of the core-hole state. The hydrogens were described using the 3*s* contracted basis of Ref. 32 with one *p*-function added.

The ground state, the core-hole state and the first valence-ionized state were self-consistently optimized—in the case of the core-hole state the occupation of the oxygen 1*s* alpha spin orbital was fixed to zero. Energies of all other valence-hole states were approximated as the ground-state energy plus the orbital energy (the energy of the Koopmans ion) with a correction given by the difference of the highest occupied molecular orbital (HOMO) orbital energy and the variationally determined HOMO ionization potential (IP). Transition dipoles for the XES were computed using the ground-state orbitals to represent both core- and valence-hole states following earlier work.[33,34] The PESs of all states were computed on a grid from 0.5 to 2.425 Å in steps of 0.025 Å; these PESs were subsequently used in all approximate methods discussed in the text.

For the simulations of the core-hole-induced dynamics classical trajectories were run for 40 fs using the STOBE code. Quantum initial conditions for the dynamics were obtained sampling the position and momentum distributions of the ground-state O-H stretch vibrational wave function since this mode is in the ground state at room temperature. For a system with more degrees of freedom the softer modes should be sampled according to a thermal ensemble. Sampling the position distribution was done by subdividing the quantum O-H stretch position probability distribution into ten distortions with equal integrated probability; the vibrational wave functions for the H-bonded and free OH were approximated as harmonic oscillators of frequency 3275 cm^{-1} and 3576 cm^{-1}, respectively, as determined for the ground-state PES (see below). The sampling of the momentum distribution was obtained by subdividing the Fourier transform similarly while accounting for the equal probability of having positive and negative momenta since the expectation value has to be zero for an initially bound system. Simulations following Odelius[5] were performed by combining a limited subset of these initial conditions since the thermal energy (k_BT) at room temperature for a classical harmonic oscillator corresponds to a significantly more limited range of initial O-H stretch distortions and initial momenta.

E. Solving the vibrational problem

The vibrational eigenfunctions were calculated using a sinc discrete variable representation (DVR).[35] A one-dimensional DVR consists of a set of basis functions $u_i(x)$ and a corresponding discrete set of DVR points x_i.[36] The functions $u_i(x)$ are localized at the corresponding points and are exactly zero on all other DVR points, i.e., $u_i(x_j)=\delta_{ij}$. The DVR basis can be used to approximately expand any one-dimensional function as $\Psi_k(x) \approx \Sigma_i c_{ki} u_i$ and is particularly useful because the localization makes it possible to approximate a matrix element of an operator depending on x as being diagonal in the basis: $\langle u_i|O(x)|u_j\rangle \approx O(x_i)\delta_{ij}$. In the sinc DVR the basis functions are

$$\sqrt{\Delta x}\frac{\sin[\pi(x-x_i)/\Delta x]}{\pi(x-x_i)} \quad (22)$$

and the corresponding DVR points form an equidistant grid $x_i = i\Delta x$, where $i=0, \pm 1, \pm 2, \ldots$ Kinetic-energy matrix elements are given by Colbert and Miller[35] as

$$T_{ij} = \frac{(-1)^{i-j}}{2m(\Delta x)^2} \begin{cases} \frac{\pi}{3} & i = j \\ \frac{2}{(i-j)^2} & i \neq j. \end{cases} \quad (23)$$

We use atomic units, $\hbar = 1$, throughout this paper. The potential energy is diagonal $V_{ij} \approx V(x_i)\delta_{ij}$. The DVR Hamiltonian $H = T + V$ is then diagonalized to obtain the eigenvectors c_{ki}. The matrix elements of an operator $O(x)$, depending on x, in this basis are given by

$$\begin{aligned} \langle \Psi_k | O(x) | \Psi_l \rangle &= \sum_i c_{ki} \langle u_i | O(x) \sum_j c_{lj} | u_{lj} \rangle \\ &= \sum_{i,j} c_{ki} c_{lj} O(x_i) \delta_{ij} \\ &= \sum_i c_{ki} c_{li} O(x_i). \end{aligned} \quad (24)$$

Since a sinc DVR basis set is associated with an equidistant grid it can be used to describe the ground-, core-ionized, and final-state vibrational wave functions on the same footing in spite of the fact that these functions, in general, are centered at different positions. The accuracy can be controlled by extending the grid and decreasing the spacing and is in practice good despite the slow decay $(1/r^2)$ of the kinetic-energy matrix. In our calculations the ground-state vibrational wave function was fully converged with respect to the DVR basis set.

F. Wave-packet dynamics on the excited state PES

At $t = 0$ we put the ground-state vibrational wave function onto the excited state PES and expand it in the excited state vibrational wave functions. After solving the vibrational problem in the sinc DVR basis the excited and ground state stretch vibrational wave functions are $|n_N\rangle = \Sigma_k b^N_{nk} |u_k\rangle$ and $|i_I\rangle = \Sigma_j c^I_{ij} |u_j\rangle$, respectively, where $|u_j\rangle$ are the DVR basis functions. Now $|u_j\rangle$ can conversely be expanded in the $|n_N\rangle$ states as $|u_j\rangle = \Sigma_n b'^N_{jn} |n_N\rangle$, where the coefficients $b'^N_{jn} = b^N_{nj} = \langle u_j | n_N \rangle$ are real. Now we can expand $|i_I\rangle$ into $|n_N\rangle$ as $|i_I\rangle = \Sigma_j c^I_{ij} |u_j\rangle = \Sigma_{j,n} c^I_{ij} b'^N_{jn} |n_N\rangle$, where the time development of $|n_N\rangle$ is given by $|n_N(t)\rangle = e^{-iE_{n_N}t} |n_N(0)\rangle$. Combining it all together gives the time development of the initial wave packet $|i_I(t)\rangle \equiv |\chi_N(t)\rangle$ as $|\chi_N(t)\rangle = \Sigma_{j,n,k} c^I_{ij} b^N_{nj} b^N_{nk} e^{-iE_{n_N}t} |u_k\rangle$ which, e.g., for DVR point l, becomes $\chi_N(x_l, t) = \Sigma_{j,n} c^I_{ij} b^N_{nj} b^N_{nl} e^{-iE_{n_N}t} u_l(x_l)$ since $u_k(x_l) = \delta_{k,l} u_l(x_l)$. Squaring this expression gives us the time-dependent probability distribution in the OH bond distance.

$$|\chi_N(x_l, t)|^2 = \left| \sum_{j,n} c^I_{ij} b^N_{nj} b^N_{nl} e^{-iE_{n_N}t} u_l(x_l) \right|^2. \quad (25)$$

III. RESULTS

We will decompose our analysis into three steps. (1) How well does a sampling of quantum initial conditions in a classical simulation capture the time-dependent probability distribution from a wave-packet simulation, (2) based on the approximated dynamics, how well do the various approximations to the spectrum calculations reproduce the KH results, and (3) how important are the energy corrections to the spectra.

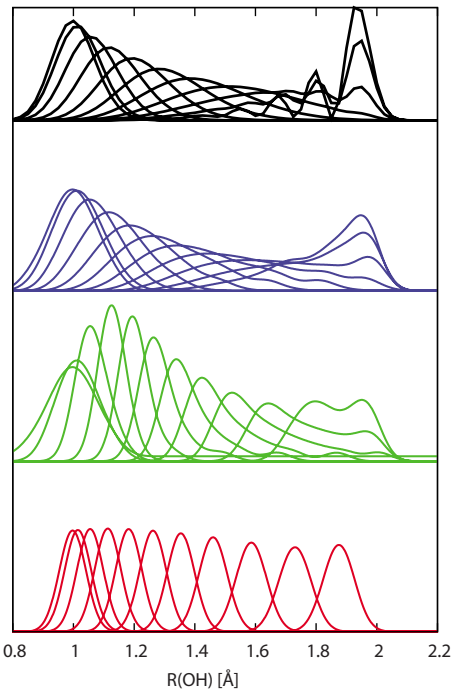

FIG. 1. (Color online) Time-dependent probability distribution of the H-bonded OH in the dimer upon nonresonant excitation with the initial state as the leftmost distribution. (a) Full quantum wave-packet dynamics, (b) classical dynamics with initial conditions sampling both the quantum distribution of OH distances and proton momenta in the zero-point motion, (c) as in (b) but sampling only the zero-point OH distance distribution, (d) classical dynamics sampling classical (thermal) initial conditions.

Here we begin by discussing the various approaches to the core-hole-induced dynamics and how they compare with the full quantum wave-packet approach in terms of the time-dependent position distribution. To evaluate the accuracy of the sampling of the quantum initial position and momentum distribution we compare the fully quantum-mechanical time-dependent probability distribution of a quantum wave packet moving on the dissociative PES, associated with the H-bonded OH upon nonresonant core ionization,[8] with the corresponding probability distributions obtained from ensembles of classical trajectories based on different initial conditions.

We first discuss approximations to the wave-packet dynamics given by $|\chi_N(x_l, t)|^2$ of Eq. (25). In Fig. 1 we compare the time-dependent position distribution from full quantum dynamics with those obtained from classical dynamics with quantum initial conditions with and without sampling the momentum distribution as well as that obtained with the time evolution of the "classical" distribution, i.e., sampling thermal conditions with vibrational energy corresponding to $k_B T$ at room temperature.[5,6] The classical dynamics based on sampling both the quantum momentum and spatial distributions as initial conditions is in very good agreement with the quantum dynamics until the wave packet reaches the accept-

ing oxygen and is reflected; the potential from the other oxygen becomes repulsive at a certain distance. When this happens the wave packet interferes with itself and nodes appear; this cannot be reproduced by the classical trajectories which correspond to the time evolution of the initial probability distribution, not of the wave-function amplitude. However, since the wave packet begins to significantly interact with the accepting oxygen only after ~7 fs interference effects from reflection of the wave packet can be expected to not affect the spectra significantly. If the distribution of momenta is neglected the agreement is less satisfactory, with the distribution actually becoming narrower for short times compared to the initial distribution, which clearly is unphysical; this is related to the gradient on the upper PES increasing for shorter internal O-H distances, which gives a larger acceleration for this part of the distribution and results in a more compact probability distribution with time. The distribution with strictly classical, thermal initial conditions, on the other hand, does not spread out almost at all with time. In this case the probability distribution moves as a unit without spreading due to the neglect of momentum sampling and since the thermal energy, ~200 cm^{-1}, of a room-temperature classical harmonic oscillator only allows sampling a very limited region of the zero-point motion of a quantized OH oscillator for which the zero-point energy is rather closer to 1800 cm^{-1}. We conclude that sampling both the space and momentum quantum distributions is necessary for a proper description of the squared wave-packet evolution and note that the agreement between the time evolution of the probability distribution using classical dynamics compared to the quantum simulation is then excellent until interference effects become important as the wave packet reaches the repulsive wall at the neighboring H-bond acceptor.

We now turn to the calculated XE spectra. For a single gas-phase water molecule there are four molecular orbitals from which electrons can decay to the 1*s* core level. Categorizing the orbitals by their symmetry and starting from the one with highest emission energy (computed in the vertical approximation, i.e., neglecting lifetime interference effects) we have the $1b_1$ lone-pair orbital (~527 eV), next comes the $3a_1$ (~524 eV) followed by the $1b_2$ (~521 eV) and $2a_1$ (~500 eV) orbitals. The nonbonding lone-pair orbital is very sharp in the experimental spectrum[1] while the bonding $3a_1$ and $1b_2$ orbitals show strong effects of core-hole-induced dynamics and become considerably broadened. The $2a_1$ orbital is around 20 eV lower in energy and is usually omitted in the spectrum. When the intermediate core-hole-state PES is dissociative, as is the case for the bonded hydrogen in the dimer, the whole spectrum can be assumed to be sensitive to the description of the dissociative dynamics but the internally bonding orbitals will show the largest effects.

In the SSCT method, full agreement with the quantum-squared wave packet will capture all the effects of the dynamics in the spectrum and will converge to the SSWPP method. The expression for the SCKH cross section, Eqs. (15) and (16), does not contain the square of the wave packet, however, so it is less certain that a sampling of initial conditions will produce an improved spectrum. Furthermore we have to investigate how large the effect of the sampling is on the spectrum since it leads to a large increase in computational effort. In Fig. 2 we show the SCKH spectra obtained with different samplings of initial conditions for the H-bonded OH. Comparing the sampling of the quantum distributions of both momenta and OH distances (a) with the strictly classical initial conditions (d) we see that quantum initial conditions improve the agreement with the full KH calculation. The inclusion of a quantum momentum sampling seems to be more important than the sampling of the position distribution; the substructure in the lone-pair peak is in better agreement when the quantum distribution of momenta is taken into account and the spatial distribution neglected (b) than when the reverse sampling is done (c). Except for this feature, the spectrum with classical initial conditions (d) does reproduce the KH spectrum qualitatively. A suitable sampling of a few points in space and momentum should thus be enough for reasonable agreement for this test system.

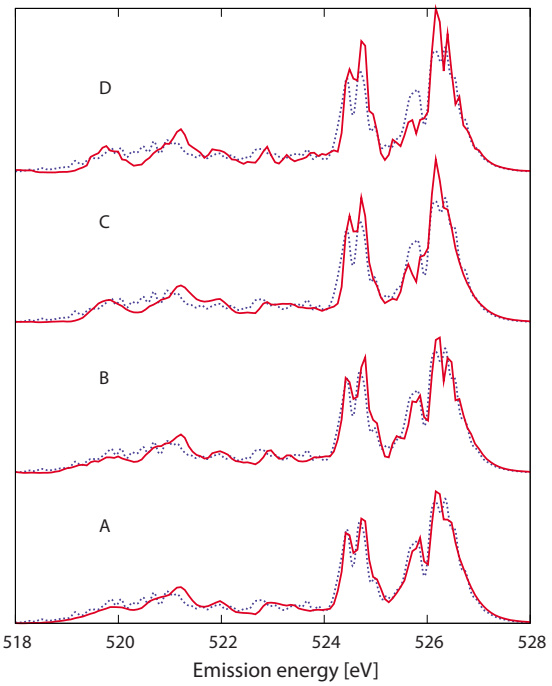

FIG. 2. (Color online) SCKH calculations for the H-bonded OH using different initial conditions for the core-hole-induced classical dynamics compared with full Kramers-Heisenberg formalism (dotted). (a) Sampling both position and momentum quantum distributions, (b) sampling quantum momentum and classical position distribution, (c) sampling classical momentum and quantum position distribution, and (d) classical initial conditions based on thermal energy only.

In Figs. 3 and 4 we show the different approximations to the XES including dynamics for, respectively, the H-bonded and non-H-bonded OH of the nonresonantly excited donor molecule. Plotted with full lines, labeled A is the SCKH, B is the SSWPP, C is the SSCT including quantum initial conditions, D is SSCT with classical initial conditions, and E is the vertical approximation; the reference KH spectrum is given by the dotted line in each plot. We see in Fig. 4 that for the non-H-bonded (free) OH all methods are in good agreement, only the peak at approximately 521 eV resolves some vibrational structure. Since the free hydrogen does not dissociate

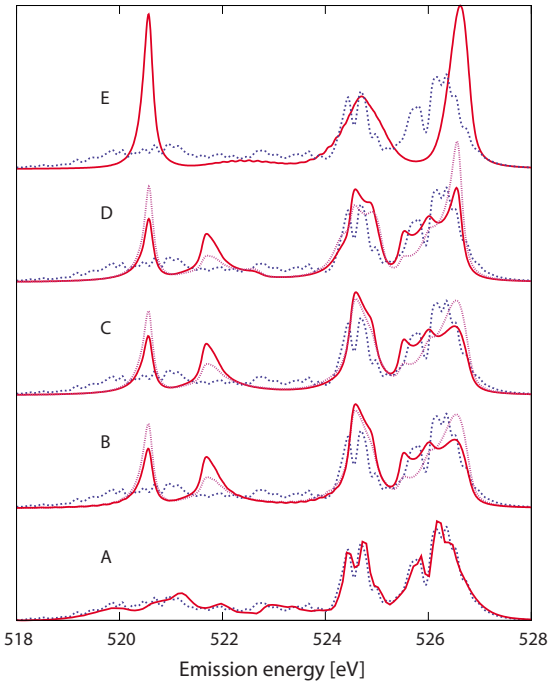

FIG. 3. (Color online) Comparison of the different methods with the full Kramers-Heisenberg formalism (blue, dotted) applied to the H-bonded OH. From bottom to top the full line represents: (a) SCKH with quantum initial conditions sampling both momentum and OH distance distributions, (b) SSWPP, (c) SSCT with quantum initial conditions, (d) SSCT with classical initial conditions, and (e) VA. In (b)–(d) the full line is spectra computed with the longer lifetime and the purple line with closely spaced dots with the shorter one.

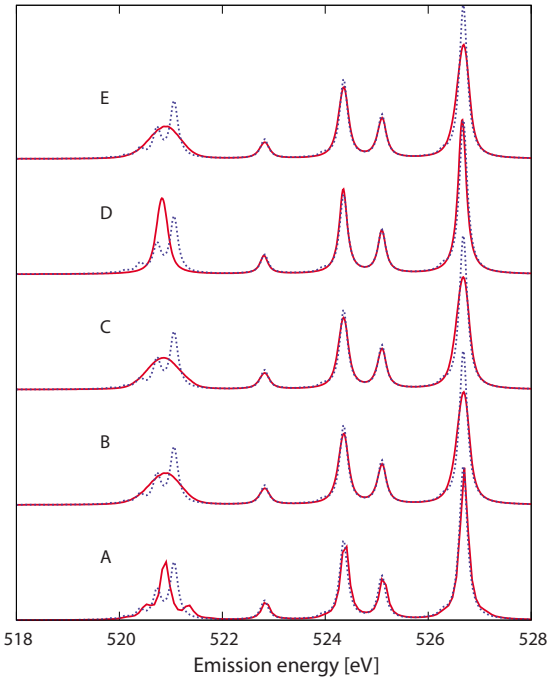

FIG. 4. (Color online) SCKH calculations for the free OH using different initial conditions for the core-hole-induced classical dynamics compared with full Kramers-Heisenberg formalism (dotted). (a) Sampling both position and momentum quantum distributions, (b) sampling quantum momentum and classical position distribution, (c) sampling classical momentum and quantum position distribution, and (d) classical initial conditions based on thermal energy only.

upon nonresonant excitation[8] there is no need for the inclusion of dynamical effects at least in this one-dimensional model system; in the case of a real system the bend modes may also contribute, even for free OH groups,[8] so dynamical effects cannot, in general, be ignored. For the H-bonded OH, however, we see large dynamical effects. If we compare the vertical approximation with KH (plot E) we see that the former has a too high and narrow lone-pair peak (around 526.5 eV) which is furthermore shifted to higher energies and lacks the vibrational structure of the KH peak. The vibrational structure in the region (518–524 eV) is totally missing in the VA spectrum, instead it shows a high and narrow peak at 520.5 eV. The SSWPP spectrum using the longer lifetime exaggerates the dynamical effect on the lone-pair peak, which is too low and broad, while the second peak is too high. In the low-emission energy region ($1b_2$) we see two smaller peaks instead of a broad distribution of intensity as obtained in the KH spectrum. With the shorter lifetime the dynamical effects in the lone-pair region are instead underestimated. We note that with a proper sampling of the initial quantum conditions we can recover the SSWPP results as seen in C. The SCKH spectrum, on the other hand, is in excellent agreement with the KH spectrum, displaying all vibrational structures of the first two peaks and near-quantitative agreement in the low-energy region. We can conclude that it is crucial to include dynamics particularly in the case of the bonded hydrogen with dissociative intermediate PES. For the free hydrogen with no dissociation the dynamics is unnecessary—even the VA method works very well. Here we need to point out that *resonant* excitation into the pre-edge feature of water or ice populates an antibonding state localized on the free OH (Refs. 37–39) leading to dissociative dynamics for the non-H-bonded OH while in that case the H-bonded OH shows only minor effects.[8] Nonresonant excitation, as studied here, instead leads to strong dynamics for the H-bonded OH such that whether or not vibrational interference and dynamical effects need to be included for a free OH depends on the excitation energy. We summarize this section by concluding that sampling the quantum initial conditions (c) reproduces the SSWPP (b), but this is not sufficient for a good agreement with the KH. The SCKH method (a), based on an ensemble of trajectories sampling the initial quantum distribution, is superior to the other approximations.

We will now discuss the PESs and the need for energy calibration. Tokushima *et al.*[2] and Pettersson *et al.*[10] pointed out the importance of the zero-point energy released in a dissociative process and in the most recent work[9] initial conditions for the classical trajectories were sampled from the ground-state vibrational OH-stretch quantum distributions in terms of both position and momentum. The spectra were calculated from the ground-state orbitals[34] but, due to difficulties in obtaining convergence of both HOMO and core IP for the large clusters used (32 molecules), a reliable absolute energy scale could not be defined and instead the energy

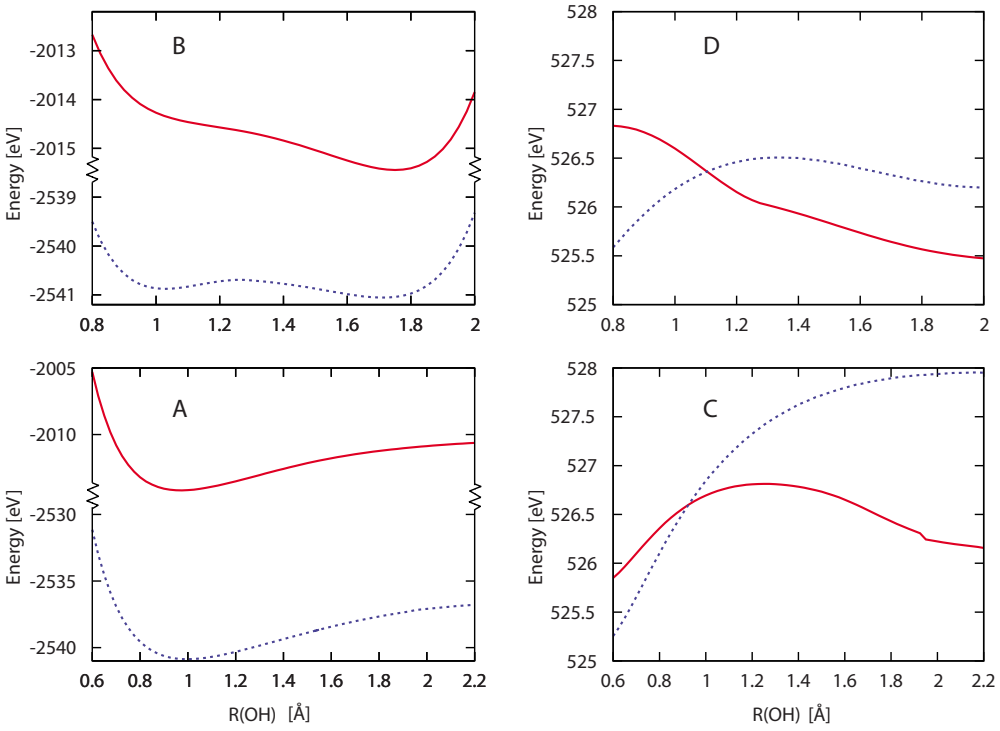

FIG. 5. (Color online) (a) and (b): PES of core-hole and lone-pair states. Full lines (red) are total energies with an explicit core hole, dotted lines (blue) are total energies with a valence hole. (a) is the free and B is the bonded hydrogen. (c) and (d): emission energies with explicit core and valence holes (red) or from orbital energy differences (blue). (c) is the free and (d) the bonded hydrogen. The orbital energies are shifted up in energy by 23.3 and 22.5 eV for the free and bonded hydrogens, respectively.

scale was taken as the orbital energy difference; using an ECP on all other oxygens in a larger cluster makes the core-hole state unique and well-defined while it proved impossible in Refs. 9 and 10 to obtain convergence for the HOMO IP in the near-degenerate lone-pair band. In Refs. 5 and 6 the initial conditions were taken from a classical MD simulation with initial momenta set to zero. An absolute energy scale was computed where the lone-pair IP was defined by eliminating orbital mixing with the remaining cluster, but these orbital mixings were subsequently included in the spectrum calculations making the energy scale less certain. Thus, also the energy scale has been an issue in all earlier work.

In Figs. 5(a) and 5(b) we show the computed PESs for the intermediate core-hole state and the lone-pair-ionized state for the free and bonded hydrogen atoms. The upper (red) and lower (blue) curves are, respectively, the PES with the explicit core hole and the PES for the lone-pair-ionized state; the core-hole PES is clearly dissociative, but even lone-pair ionization affects the PES leading to a double-well potential with a small barrier (~0.2 eV) separating the molecular from the deeper dissociated minimum. For the free hydrogen [Fig. 5(a)] neither PES is dissociative. Here it should be remembered that all other atoms are fixed in these one-dimensional simulations such that the depth of the dissociated minimum can be expected to increase if also the hydrogen atoms of the accepting water were allowed to relax.

The resulting emission energies as function of the respective OH-stretch coordinate are shown in Figs. 5(c) and 5(d) in comparison to a simple estimate based on the orbital energy differences. The latter was shifted in energy to make the first peak of the spectra coincide (as in Fig. 6). At longer distances, and thus longer times in terms of the wave-packet dynamics, the emission position of the H-bonded OH, based on the orbital energy difference and the fully computed, show very similar and near-parallel behavior. At shorter times, however, the two curves are qualitatively different; the fully computed curve shows reduced emission energy with elongation while the estimate based on orbital energies shows an increase up to an OH distance of 1.2 Å. With an OH equilibrium distance in the ground state of 1.00 Å for the H-bonded OH it is clear that the lone-pair peak based on orbital energy differences will come out too sharp and narrow and lack the asymmetry toward lower emission energy that is evident from the distance dependence of the fully energy-corrected emission energy curve. The situation is similar for the free OH but with smaller variations with the orbital energy difference giving an asymmetry toward higher emission energy; since there is no dissociation only a smaller region around the equilibrium will furthermore be probed. In Fig. 6 we show SCKH spectra for the free and H-bonded OH using different energy calibrations comparing the fully corrected case to spectra using transition energies either taken from the ground-state orbital-energy differences (no correction, as in Refs. 9 and 10) or just correcting for the core-hole state which gives the dominant effect.

The spectra have been shifted to the fully corrected position to be able to compare their shapes; the shifts were +23.3 eV for the uncorrected spectrum and −4.7 eV for the spectrum only corrected for the core-hole energy. For the

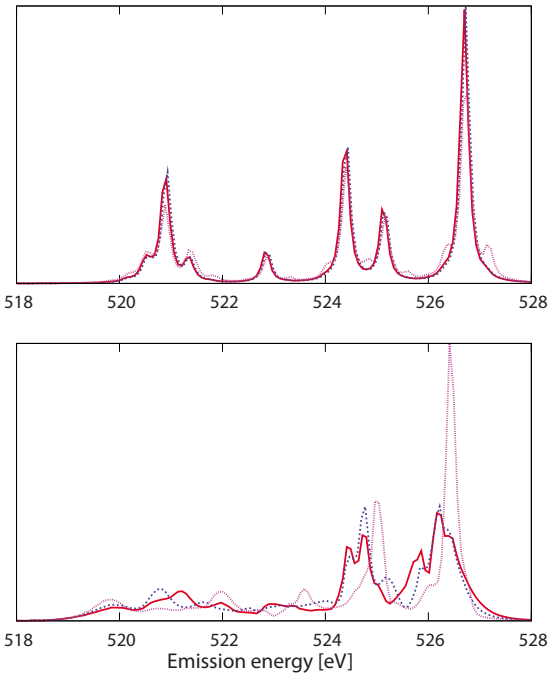

FIG. 6. (Color online) Sensitivity to energy calibration in the SCKH method. Upper: free hydrogen, lower: bonded hydrogen. Full line: core hole and lone pair corrected, dotted line: only core hole corrected, and line with closely spaced dots: no corrections. The spectra have been shifted to make the first peak (lone pair) coincide, which means 23.3 eV for the free and 22.5 eV for the bonded hydrogen, respectively.

free hydrogen the energy corrections do not affect the shape much but including the core-hole correction improves the spectrum somewhat to almost coincide with the fully corrected one. For the H-bonded OH the core-hole correction is crucial—the lone-pair peak is much too high and narrow without it, as is now seen to have been the case in Ref. 10. The same is the case for the second peak. For the free hydrogen, on the other hand, the core-hole correction gives a higher and sharper peak.

IV. CONCLUSIONS

We have developed a semiclassical approximation (SCKH) to the Kramers-Heisenberg formula for nonresonant XES that gives excellent agreement with the quantum Kramers-Heisenberg spectrum for our 1D water dimer model system. Upon nonresonant core excitation the H-bonded hydrogen shows strong dynamical and vibrational interference effects which are crucial for a reliable representation of the spectrum; these are included through a summation over trajectories based on classical Born-Oppenheimer dynamics sampling both the initial position and momentum quantum distributions as initial condition for the core-hole-induced dynamics. The SCKH formula gives superior agreement compared to the methods of Tokushima *et al.*[2,9,10] and Odelius[5,6] (the SSCT method as defined above) for this test system, and it also has a more rigorous theoretical foundation. We finally note that, on the time-scale relevant for the core hole, the time development of the O-H probability distribution from classical mechanics closely parallels that of the quantum-mechanical wave packet once a proper sampling of the initial quantum distribution of internal distances and momenta is used as initial conditions for the core-hole-induced dynamics as in Refs. 9 and 10.

Hence, we can finally settle the question about the importance of quantum initial conditions in XES calculations that have been under debate.[2,5,6,9,10] However, more importantly, we conclude that the SSCT method is not sufficient to reproduce the KH spectrum, regardless of the initial conditions used. Although it seems likely that the large spread in initial conditions should lead to a smearing out of sharp spectral features in computed spectra, as has been suggested in Refs. 2, 9, and 10, it is necessary to apply the here derived SCKH approximation to reinvestigate the effects using more realistic models of liquid water.

ACKNOWLEDGMENTS

This work was supported by the Swedish Natural Science Research Council, the EU FP7 HYPOMAP network and by the National Science Foundation (U.S.) under Grant No. CHE-0809324. M.P.L. acknowledges a generous grant from Lennanders Foundation. Generous grants of computer time at the Swedish National Supercomputer Center as well as stimulating discussions with Andreas Koster, CINVESTAV, and Faris Gel'mukhanov, KTH, are gratefully acknowledged.

APPENDIX A: THE KRAMERS-HEISENBERG FORMULA, FROM THE RESONANT TO THE NONRESONANT CASE

The Kramers-Heisenberg formula for the general case treating both incoming and outgoing radiation is[11,15]

$$\sigma(\omega,\omega') = \sum_f \left| \sum_n \frac{\langle f|D'|n\rangle\langle n|D|i\rangle}{\omega' - E_{nf} + i\Gamma} \right|^2 \Phi(\omega - \omega' - E_{fi}, \gamma), \tag{A1}$$

where now ω denotes the frequency of the incoming radiation and Φ is an instrumental broadening function with HWHM γ. When an electron is promoted to the continuum, which is the case for nonresonant transitions, we write the wave function as $|n\rangle = |n'\rangle|\varepsilon_n\rangle$ and $|f\rangle = |f'\rangle|\varepsilon_f\rangle$ where the primed wave functions are the remaining bound state and $|\varepsilon\rangle$ is the wave function of the outgoing electron, labeled by its energy. Energies become $E_f = E_{f'} + \varepsilon_f$ and $E_n = E_{n'} + \varepsilon_n$, sums over states become $\Sigma_f = \Sigma_{f'} \int d\varepsilon_f$ and $\Sigma_n = \Sigma_{n'} \int d\varepsilon_n$. We thus have

$$\sigma(\omega,\omega') = \sum_{f'} \int d\varepsilon_f \times \left| \sum_{n'} \int d\varepsilon_n \frac{\langle \varepsilon_f|\langle f'|D'|n'\rangle|\varepsilon_n\rangle\langle \varepsilon_n|\langle n'|D|i\rangle}{\omega' - E_{n'f'} - \varepsilon_n + \varepsilon_f + i\Gamma} \right|^2 \times \Phi(\omega - \omega' - E_{f'i} - \varepsilon_f, \gamma). \tag{A2}$$

The transition dipole operator can be written as $D = D_{N-1}$

$+D_{pe}$ where the first part comes from the $N-1$ electrons in the remaining ion and the second from the photoelectron. Using this we can separate the transition dipole matrix element as

$$\begin{aligned}\langle \varepsilon_f | \langle f' | D_{N-1} + D_{pe} | n' \rangle | \varepsilon_n \rangle \\ = \langle \varepsilon_f | \varepsilon_n \rangle \langle f' | D_{N-1} | n' \rangle + \langle \varepsilon_f | D_{pe} | \varepsilon_n \rangle \langle f' | n' \rangle \\ \approx \delta(\varepsilon_f - \varepsilon_n) \langle f' | D_{N-1} | n' \rangle, \end{aligned} \tag{A3}$$

where in the last step we assume that only the first term contributes, that is that there are no transitions for the photoelectron. Performing the integral over ε_n picks out the value of the integrand where $\varepsilon_f = \varepsilon_n$ due to the delta function. This gives

$$\begin{aligned}\sigma(\omega, \omega') \propto \sum_{f'} \int d\varepsilon_f \left| \sum_{n'} \frac{\langle f' | D' | n' \rangle \langle \varepsilon_n | \langle n' | D | i \rangle}{\omega' - E_{n'f'} + i\Gamma} \right|^2 \\ \times \Phi(\omega - \omega' - E_{f'i} - \varepsilon_f, \gamma). \end{aligned} \tag{A4}$$

If we assume that the transition dipole matrix element between initial and intermediate states is independent of ε_f the whole expression is independent of ε_f. The integral is then just over the broadening function which gives a constant, one if it is normalized. In the following we do not write out the wave function of the photoelectron, assuming implicitly that the transition dipole between intermediate and final states is between the remaining ion states and that the photoelectron should be included in the matrix element between initial and intermediate states (the last one, however, is often assumed to be a constant). We then end up with the expression for the nonresonant cross section applicable to cases where the intermediate state is core ionized and the interaction with the emitted photoelectron can be neglected

$$\sigma(\omega') \propto \sum_{f} \left| \sum_{n} \frac{\langle f | D' | n \rangle \langle n | D | i \rangle}{\omega' - E_{nf} + i\Gamma} \right|^2. \tag{A5}$$

APPENDIX B: A NOTE ON THE LIFETIME

An energy eigenstate $|i\rangle$ has the time development

$$|i(t)\rangle = c_i(t) |i(0)\rangle \tag{B1}$$

with

$$c_i(t) = e^{-i(E_i/\hbar)t}. \tag{B2}$$

If the state has a finite lifetime there will also be a factor of $e^{-(\Gamma/\hbar)t}$ in $c_i(t)$. We thus have

$$c_i(t) = e^{-i(E_i/\hbar)t} e^{-(\Gamma/\hbar)t}. \tag{B3}$$

Fourier transforming this expression gives a Lorentzian instead of a delta function; the energy of the state is now uncertain. To identify Γ we Fourier transform the Lorentzian lifetime broadening

$$\frac{1}{2\pi} \int_{-\infty}^{\infty} \frac{2\Gamma}{(\hbar\omega - E_i)^2 + \Gamma^2} e^{-i\omega t} d\omega = \frac{1}{\hbar} e^{-i(E_i/\hbar)t} e^{-(\Gamma/\hbar)|t|} \tag{B4}$$

which shows that Γ is the HWHM of the Lorentzian (assuming positive times). The square of $c_i(t)$ is the time-dependent probability to find the system in state $|i\rangle$

$$|c_i(t)|^2 = e^{-2(\Gamma/\hbar)t} = e^{-t/\tau}, \tag{B5}$$

where the lifetime τ has been introduced as the decay constant of the probability and is defined as $\tau = \frac{\hbar}{2\Gamma}$ or $\tau = \frac{\hbar}{\Gamma'}$ with Γ' being the FWHM broadening. This means that we can write $c_i(t) = e^{-i(E_i/\hbar)t} e^{-t/2\tau}$ in terms of the lifetime defined above. Thus, a factor of 2 is to be used in the denominator in the exponent for $c_i(t)$ (but not for $|c_i(t)|^2$). In the formulas for the absorption and emission processes we only encounter factors of $e^{-(\Gamma/\hbar)t}$ which translates into $e^{-t/2\tau}$. The approach of Refs. 2 and 7–10 considered the decay of a state at a specified time t with the population of the state decreased through earlier decay processes. This lead to the use of the factor $e^{-t/\tau}$. Since the SSCT (and SSWPP) methods are not rigorous approximations to the KH formula the question of which lifetime to use becomes a bit arbitrary. The core-hole clock method[40–45] is used to determine ratios of lifetimes (or Γ parameters) between spectator and nonspectator decay channels, as shown in Ref. 41. If one is consistent in the definition of the lifetimes then this method is not affected by a possible factor of 2.

[1] O. Fuchs, M. Zharnikov, L. Weinhardt, M. Blum, M. Weigand, Y. Zubavichus, M. Bär, F. Maier, J. D. Denlinger, C. Heske, M. Grunze, and E. Umbach, Phys. Rev. Lett. **100**, 027801 (2008).

[2] T. Tokushima, Y. Harada, O. Takahashi, Y. Senba, H. Ohashi, L. G. M. Pettersson, A. Nilsson, and S. Shin, Chem. Phys. Lett. **460**, 387 (2008).

[3] J. Forsberg, J. Gråsjö, B. Brena, J. Nordgren, L.-C. Duda, and J.-E. Rubensson, Phys. Rev. B **79**, 132203 (2009).

[4] C. Huang, K. T. Wikfeldt, T. Tokushima, D. Nordlund, Y. Harada, U. Bergmann, M. Niebuhr, T. M. Weiss, Y. Horikawa, M. Leetmaa, M. P. Ljungberg, O. Takahashi, A. Lenz, L. Ojamäe, A. P. Lyubartsev, S. Shin, L. G. M. Pettersson, and A. Nilsson, Proc. Natl. Acad. Sci. U.S.A. **106**, 15214 (2009).

[5] M. Odelius, Phys. Rev. B **79**, 144204 (2009).

[6] M. Odelius, J. Phys. Chem. A **113**, 8176 (2009).

[7] B. Brena, D. Nordlund, M. Odelius, H. Ogasawara, A. Nilsson, and L. G. M. Pettersson, Phys. Rev. Lett. **93**, 148302 (2004).

[8] M. Odelius, H. Ogasawara, D. Nordlund, O. Fuchs, L. Weinhardt, F. Maier, E. Umbach, C. Heske, Y. Zubavichus, M. Grunze, J. D. Denlinger, L. G. M. Pettersson, and A. Nilsson, Phys. Rev. Lett. **94**, 227401 (2005).

[9] T. Tokushima, Y. Harada, Y. Horikawa, O. Takahashi, Y. Senba, H. Ohashi, L. G. M. Pettersson, A. Nilsson, and S. Shin, J. Electron Spectrosc. Relat. Phenom. **177**, 192 (2010).

[10] L. G. M. Pettersson, T. Tokushima, Y. Harada, O. Takahashi, S. Shin, and A. Nilsson, Phys. Rev. Lett. **100**, 249801 (2008).

[11] F. Gel'mukhanov and H. Ågren, Phys. Rep. **312**, 87 (1999).
[12] J. Sakurai, *Advanced Quantum Mechanics* (Addison-Wesley, Menlo Park, CA, 1967).
[13] M. Eroms, O. Vendrell, M. Jungen, H. D. Meyer, and L. S. Cederbaum, J. Chem. Phys. **130**, 154307 (2009).
[14] H. D. Meyer, U. Manthe, and L. S. Cederbaum, Chem. Phys. Lett. **165**, 73 (1990).
[15] F. K. Gel'Mukhanov, L. N. Mazalov, and A. V. Kondratenko, Chem. Phys. Lett. **46**, 133 (1977).
[16] D. W. Oxtoby, D. Levesque, and J. J. Weis, J. Chem. Phys. **68**, 5528 (1978).
[17] S. Mukamel, J. Chem. Phys. **77**, 173 (1982).
[18] S. Mukamel, *Principles of Nonlinear Optical Spectroscopy* (Oxford University Press, New York, 1995).
[19] F. Gel'mukhanov and H. Ågren, Phys. Rev. A **49**, 4378 (1994).
[20] M. P. Ljungberg, L. G. M. Pettersson, and A. Nilsson (unpublished).
[21] A. Nilsson and L. G. M. Pettersson, Surf. Sci. Rep. **55**, 49 (2004).
[22] P. Sałek, F. Gel'mukhanov, and H. Ågren, Phys. Rev. A **59**, 1147 (1999).
[23] M. Neeb, J. E. Rubensson, M. Biermann, and W. Eberhardt, J. Electron Spectrosc. Relat. Phenom. **67**, 261 (1994).
[24] S. L. Sorensen, R. Fink, R. Feifel, M. N. Piancastelli, M. Bässler, C. Miron, H. Wang, I. Hjelte, O. Björneholm, and S. Svensson, Phys. Rev. A **64**, 012719 (2001).
[25] H. A. Harker, F. N. Keutsch, C. Leforestier, Y. Scribano, J.-X. Han, and R. J. Saykally, Mol. Phys. **105**, 497 (2007).
[26] V. C. Felicissimo, I. Minkov, F. F. Guimarães, F. Gel'mukhanov, A. Cesar, and H. Ågren, Chem. Phys. **312**, 311 (2005).
[27] V. C. Felicíssimo, F. F. Guimarães, F. Gel'mukhanov, A. Cesar, and H. Ågren, J. Chem. Phys. **122**, 094319 (2005).
[28] K. Hermann, L. G. M. Pettersson, M. E. Casida, C. Daul, A. Goursot, A. Koester, E. Proynov, A. St-Amant, D. R. Salahub, V. Carravetta, A. Duarte, N. Godbout, J. Guan, C. Jamorski, M. Leboeuf, M. Leetmaa, M. Nyberg, L. Pedocchi, F. Sim, L. Triguero, and A. Vela, DEMON software, Stockholm-Berlin, 2005.
[29] J. P. Perdew, K. Burke, and M. Ernzerhof, Phys. Rev. Lett. **77**, 3865 (1996).
[30] W. Kutzelnigg, U. Fleischer, and M. Schindler, *NMR: Basic Principles and Progress* (Springer-Verlag, Heidelberg, 1990).
[31] L. G. M. Pettersson, U. Wahlgren, and O. Gropen, J. Chem. Phys. **86**, 2176 (1987).
[32] S. Huzinaga, J. Chem. Phys. **42**, 1293 (1965).
[33] L. Triguero, L. G. M. Pettersson, and H. Ågren, J. Phys. Chem. **102**, 10599 (1998).
[34] A. Föhlisch, J. Hasselström, P. Bennich, N. Wassdahl, O. Karis, A. Nilsson, L. Triguero, M. Nyberg, and L. G. M. Pettersson, Phys. Rev. B **61**, 16229 (2000).
[35] D. T. Colbert and W. H. Miller, J. Chem. Phys. **96**, 1982 (1992).
[36] J. C. Light and T. Carrington, Adv. Chem. Phys. **114**, 263 (2000).
[37] M. Cavalleri, H. Ogasawara, L. G. M. Pettersson, and A. Nilsson, Chem. Phys. Lett. **364**, 363 (2002).
[38] Ph. Wernet, D. Nordlund, U. Bergmann, M. Cavalleri, M. Odelius, H. Ogasawara, L. Å. Näslund, T. K. Hirsch, L. Ojamäe, P. Glatzel, L. G. M. Pettersson, and A. Nilsson, Science **304**, 995 (2004).
[39] D. Nordlund, H. Ogasawara, H. Bluhm, O. Takahashi, M. Odelius, M. Nagasono, L. G. M. Pettersson, and A. Nilsson, Phys. Rev. Lett. **99**, 217406 (2007).
[40] O. Björneholm, A. Nilsson, A. Sandell, B. Hernnäs, and N. Mårtensson, Phys. Rev. Lett. **68**, 1892 (1992).
[41] M. Ohno, Phys. Rev. B **50**, 2566 (1994).
[42] O. Karis, A. Nilsson, M. Weinelt, T. Wiell, C. Puglia, N. Wassdahl, N. Mårtensson, M. Samant, and J. Stöhr, Phys. Rev. Lett. **76**, 1380 (1996).
[43] W. Wurth and D. Menzel, Chem. Phys. **251**, 141 (2000).
[44] A. Föhlisch, P. Feulner, F. Hennies, A. Fink, D. Menzel, D. Sanchez-Portal, P. M. Echenique, and W. Wurth, Nature (London) **436**, 373 (2005).
[45] P. A. Brühwiler, O. Karis, and N. Mårtensson, Rev. Mod. Phys. **74**, 703 (2002).